Electronic Supplementary Material (ESI) for Materials Horizons.

Electronic Supplementary Information

Oligoanilines as a Suppressor of Polysulfide Shuttling in Lithium-Sulfur Batteries

*Chi-Hao Chang, Sheng-Heng Chung, Pauline Han, and Arumugam Manthiram**

C.-H. Chang, S.-H. Chung, P. Han, Prof. A. Manthiram
Materials Science and Engineering Program & Texas Materials Institute
The University of Texas at Austin, Austin, TX 78712, USA
E-mail: manth@austin.utexas.edu (A. Manthiram)

Synthesis of amine-capped aniline trimer (ACAT): As analogues of the well-known polyaniline (PANi), aniline oligomers, especially ACAT, have been extensively studied because of their well-defined structure and good solubility. A simple one-step method was well-established recently by Yeh *et al.* to prepare ACAT in a large scale and at low cost.[1–5] Briefly, ACAT was synthesized by the oxidative coupling reaction of 4,4'-diaminodiphenylamine sulfate (TCI) and distilled aniline (Sigma-Aldrich) with ammonium persulfate (APS, JT Baker) as an oxidant at -5 ^{o}C (Fig. S1a). The resulting products were obtained by the vacuum-filtration method and then washed with 1.0 M hydrogen chloride (HCl, Sigma-Aldrich) solution. The HCl-doped ACAT was subsequently dedoped by ammonium hydroxide solution (NH_4OH, Sigma-Aldrich) and continually washed by a huge amount of purified H_2O. The purple-blue ACAT powders were obtained after vacuum-drying at 50 ^{o}C for 24 h. The characterizations of ACAT are presented in Fig. S1b – d.[6] ^{1}H NMR (300 MHz, d$_6$-DMSO, ppm): δ = 5.43 (1, 4H, -NH_2), δ = 6.61 (2, 4H, Ar-H), δ = 6.75 (3, 4H, Ar-H), δ = 6.94 (4, 4H, Ar-H). Mass: $[ACAT+H]^+ = 289.1$. FTIR (KBr pellets, cm^{-1}): 3306 and 3202 (terminal -NH_2), 1602 (quinoid rings), 1506 (benzenoid rings), 1283 (C-N), 838 (*para*-substitution of benzene ring).

Synthesis of polyaniline (PANi): In a typical synthesis procedure,[7] 0.1 mole of distilled aniline monomers were added into 400 mL of 1.0 M HCl solution and the mixture was precooled in an ice bath. A 20 mL of 1.0 M HCl solution containing 0.025 mol APS was added into the above aniline/HCl solution dropwise. The mixture was kept under -5 °C with vigorous magnetic stirring for 6 h. The HCl-doped PANi was obtained by vacuum-filtering the resulting solutions. To convert the HCl-doped PANi to the emeraldine PANi (or dedoped PANi), the HCl-doped PANi precipitates were magnetically stirred in 400 mL NH_4OH (1.0 M) solution at room temperature for 24 h. The emeraldine PANi powders were obtained by the vacuum-filtration method and vacuum-drying at 50 ^oC.

The solubility examinations: 5 mg ACAT or PANi powders were dissolved in various electrolyte solvents (8 mL) such as 1, 3-dioxolane (DOL, Acros Organics), 1,2-dimethoxyethane (DME, Acros Organics), and the DOL/DME co-solvent. The solutions were stirred at room temperature for 1 day.

Preparation of $LiNO_3$- and ACAT/$LiNO_3$-electrolytes: The $LiNO_3$-electrolyte was prepared by completely dissolving the lithium salt (1.85 M, $LiCF_3SO_3$, Acros Organics) and the electrolyte additive (0.1 M, $LiNO_3$, Acros Organics) in the DOL/DME co-solvent. The ACAT/$LiNO_3$-electrolyte was obtained by introducing 0.05 M of the as-synthesized ACAT into the $LiNO_3$-electrolyte. The ACAT/$LiNO_3$-electrolyte is purple-blue in color; the $LiNO_3$-electrolyte, however, is transparent.

Fabrication of sulfur cathodes: The pure sulfur cathodes with two different sulfur contents (60 wt.% sulfur denoted as 60S-cathodes and 70 wt.% sulfur denoted as 70S-cathodes) were prepared by coating the active-material slurry onto an aluminum foil (the current collector). The slurry containing 60 wt.% pure sulfur powders (S, Sigma-Aldrich), 20 wt.% polyvinylidene fluoride (PVdF, Kureha), and 20 wt.% Super P (TIMCAL) in N-methyl-2-pyrrolidone (NMP, Sigma-Aldrich) were employed to prepare the 60S-cathodes. On the other hand, the slurry composed of 70 wt.% sulfur, 15 wt.% PVdF, and 15 wt.% Super P was used in the preparation of the 70S-cahtodes. The wet cathodes were vacuum-dried in an oven at 50 ^{o}C for 24 h to vaporize the NMP solvent and any residual moisture. The sulfur loading of the prepared 60S-cathodes is approximately 2.0 – 2.2 mg cm^{-2}. The sulfur loadings of the prepared 70S-cathodes were tuned from 2.2 to 5.1 mg cm^{-2} by controlling the thickness of the active-material coating.

Preparation of the modified cathodes: 1.0 M Li_2S_6 prepared by a chemical reaction of pure sulfur powders and Li_2S powders at 75 ^{o}C was used as the active material in the modified cathode. 30 μL Li_2S_6 solution was dropped onto a highly conductive carbon paper, which functionalizes as a porous current collector. The resulting cathode contains *ca.* 5.1 mg cm^{-2}/72 wt.% sulfur.

Preparation of the carbon-coated separators: The carbon-coated separators have been well-established in our group.[8–11] In this work, porous carbon spheres (PCS) and single-walled carbon nanotubes (SWCNT, Tuball) were used as the coating materials in the carbon-coated separators. The carbon-coated separators were fabricated by vacuum-filtering the isopropyl alcohol (IPA, Fisher Scientific) solution containing 0.25 mg mL^{-1} PCSs and 0.05 mg mL^{-1} SWCNTs through the polymeric separator (Celgard®2500, Celgard). The resulting carbon-coated separators were vacuum-dried at 50 °C for 24 h. The coated side faced the sulfur cathode when assembling the Li-S cells with the carbon-coated separators. The other side facing the Li anode remained insulating, preventing the cells from short-circuiting. The weight of carbon coating is about 0.12 mg cm^{-2}. As a reference, the Celgard separator is ca. 1.0 mg cm^{-2}.

Ex-situ and in-situ LiPS permeation: 0.2 mL of the 1 M Li_2S_6 solution prepared through a chemical reaction of pure sulfur powders and Li_2S powders at 75 ^{o}C mixed with 1 mL of the electrolytes ($LiNO_3$-electrolyte or ACAT/$LiNO_3$-electrolyte) was transferred to into a small sample vial. The outlet of the small sample vials with the solutions was sealed by the separators (polymeric separators or carbon-coated separators). The well-sealed vials with the solutions were then transferred upside down into the large sample vials containing 2.0 mL $LiNO_3$-electrolyte. The solutions in the small vials would gradually diffuse into the electrolyte in the large vials due to the concentration differences. The permeability was quantitatively determined by UV-Vis spectroscopy after different diffusing times of 30 min, 1 h, and 3 h.

In the LiPS-trap cells used to perform the *in-situ* permeation test, a sheet of sulfur-free carbon paper (Nanotech) was placed between two polymeric separators. We also replaced the top polymeric separator with the carbon-coated separator in the LiPS-trap cells in order to investigate the further reduced migration of LiPS. The inserted porous carbon papers exhibit intertwined porous structures and thereby function as LiPS traps to confine the migrating LiPS escaping from the sulfur cathode. After cycling, the cycled carbon papers (at the fully charged stage, 2.8 V) were retrieved from the cells and rinsed with DOL/DME to remove the remaining Li salts. The SEM images and the elemental mapping results of the surface facing the sulfur cathode of the cycled carbon papers were used to quantitatively examine the amount of the escaped LiPS from the sulfur cathodes.

Characterizations: The microstructural/morphological analyses and the elemental mapping investigations were observed with a field emission scanning electron microscope (FE-SEM) (Quanta 650 FE-SEM, FEI) equipped with an energy dispersive X-ray spectrometer (EDX). The samples retrieved from the cycled cells were slightly rinsed with the DOL/DME solution. In order to prevent contact with air, the cycled samples were transferred in vials containing ultra-high pure argon. The bonding states and the chemical characterizations of ACAT powders, ACAT-LiPS complexes, and cycled cathodes were examined with X-ray photoelectron spectroscopy (XPS, Axis Ultra DLD, Kratos Analytical) equipped with a monochromated Al

Kα X-ray source. A specially-designed air-tight chamber developed by the Texas Materials Institute was used to transfer the air-sensitive samples. To eliminate the interferences of Li salts (e.g., $LiCF_3SO_3$ and $LiNO_3$) in the XPS analyses, the LiPS mixtures used to prepare the ACAT-LiPS complexes were prepared by mixing sulfur powders and Li_2S powders in the DOL/DME co-solvent without involving any Li salts at 75°C. The LiPS mixtures were obtained by filtering out the unreacted S/Li_2S powders. UV-Vis absorption spectra were obtained with a UV-Vis spectrometer (Ocean Optics, Halogen light source, UV-NIR). Fourier transformed infrared (FT-IR) spectra were recorded on a FT-IR spectrometer (Nicolet iS5) in the wavenumber range of 500 to 4000 cm^{-1}. The porosity analysis was carried out by examining the nitrogen adsorption and desorption behaviors of the samples with an automated gas sorption apparatus (AutoSorb iQ2, Quantachrome Instruments) at -196 °C.

Electrochemical Measurements: The assembled Li-S cells were rested for 30 min prior to the electrochemical examinations performed at room temperature. A universal potentiostat (VoltaLab PGZ 402, Radiometer Analytical) was used for the cyclic voltammetry (CV) measurement between the voltages of 1.7 and 2.8 V. The electrochemical performances and the discharge/charge voltage profiles were collected with an Arbin electrochemical test station in the voltage range of 1.7 – 2.8 V. The upper-discharge plateau capacity (Q_H) and the lower-discharge plateau capacity (Q_L) were based on the discharge curves.

Supplementary Figures, Tables, and Discussions

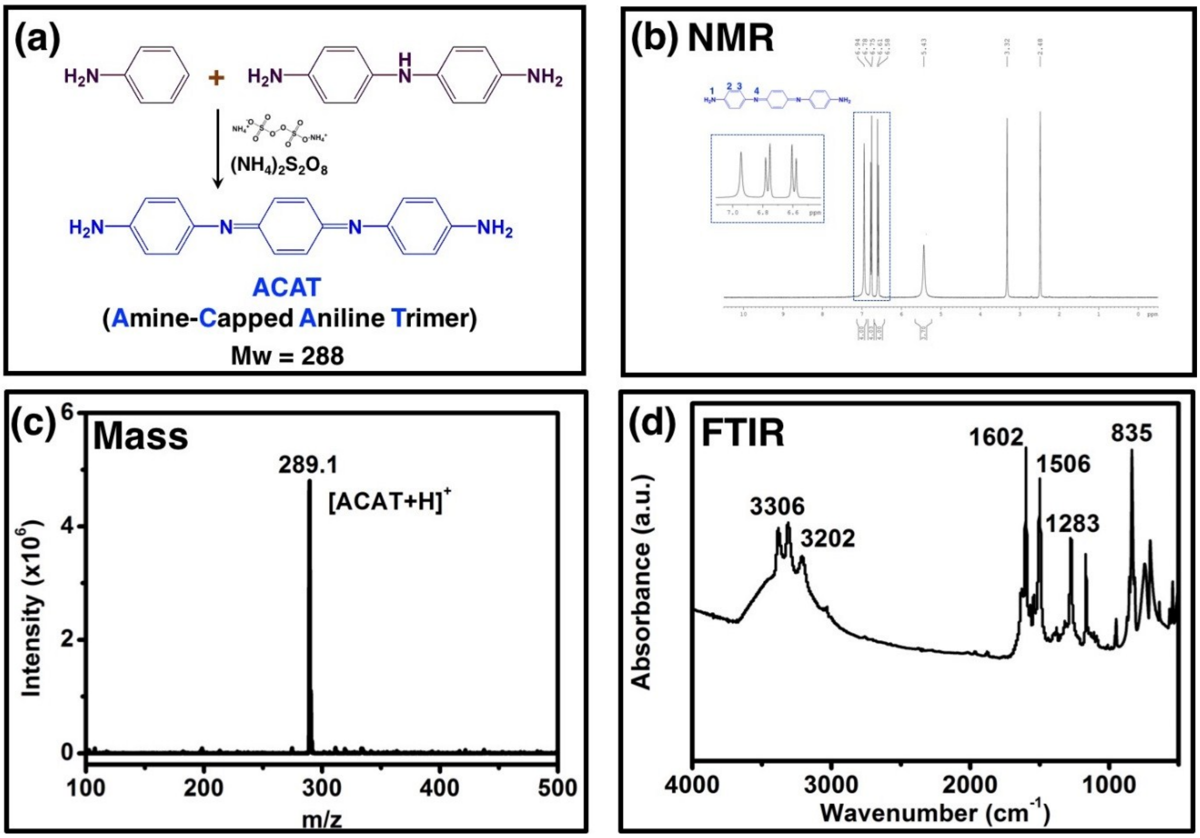

Fig. S1 (a) Scheme for the synthesis of ACAT. Characterizations of ACAT: (b) ^{1}H NMR, (c) mass spectrum, and (d) FTIR spectrum.

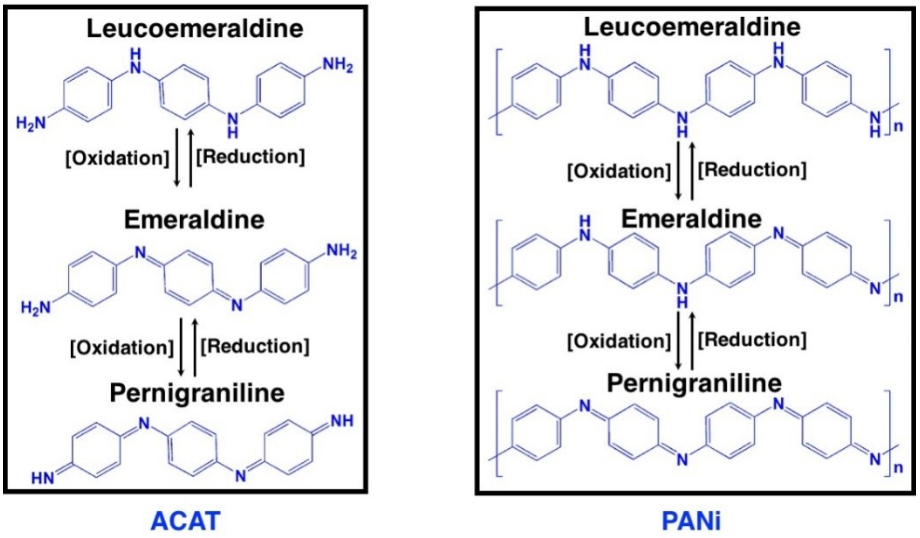

Fig. S2 Chemical structures and the various redox states of ACAT and PANi.

Fig. S2 presents the basic redox reactions of ACAT and PANi. Similar to PANi, the leucomeraldine ACAT (the fully reduced form) can be oxidized to the emeraldine ACAT (the half-oxidized form), which is the relatively stable form.[3,12–14] The emeraldine ACAT is able to further transform into the pernigraniline ACAT (the fully oxidized form). Sharing the same chemical structures, the ACAT molecules also exhibit strong interactions with LiPS, as discussed in the XPS and UV-Vis results.

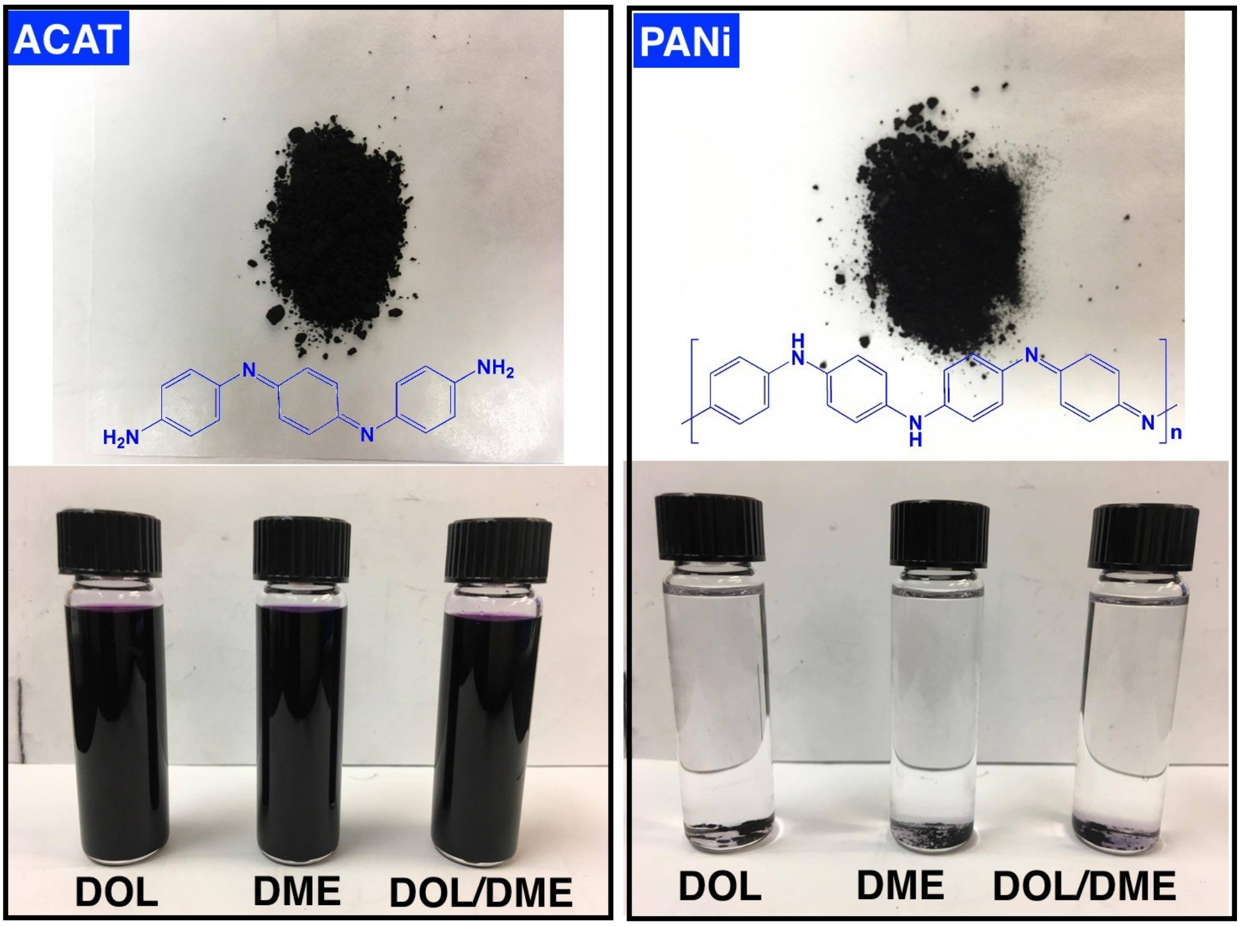

Fig. S3 Solubility tests of ACAT and PANi.

Because PANi is a conjugated polymer with a rigid aromatic chemical structure and high molecular weight,[14,15] it hardly dissolves in any solvents. The most common solvent for PANi is NMP. Unlike PANi, the oligo-derivative of PANi, ACAT, exhibits excellent solubility in the electrolyte solvents including DOL, DME, and DOL/DME co-solvent (Fig. S3). ACAT, in fact, is also highly soluble in many common solvents such as ethanol, acetone, and isopropanol. As a result of the excellent solubility of ACAT, we are able to adopt ACAT as an electrolyte co-additive.

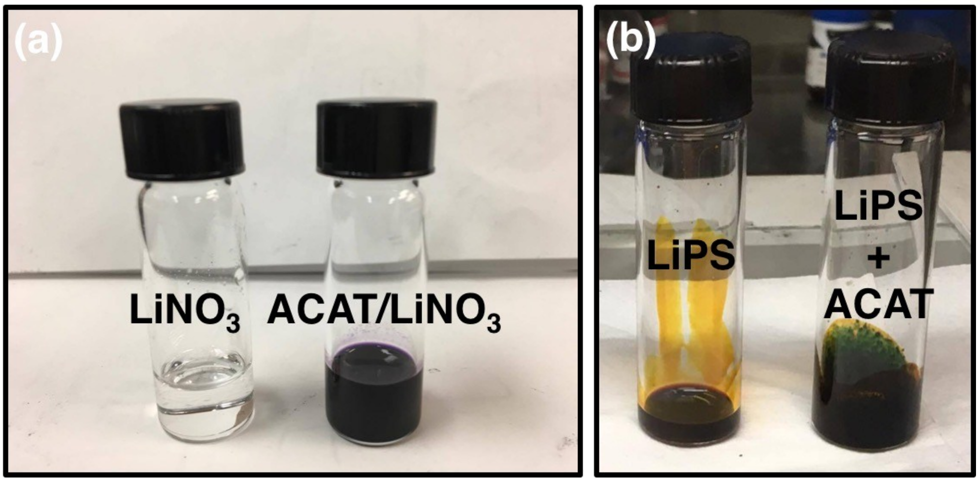

Fig. S4 Photos of (a) LiNO$_3$-electrolyte and ACAT/LiNO$_3$-electrolyte; (b) LiPS and LiPS/ACAT mixtures.

LiNO$_3$-electrolyte is transparent and colorless; the electrolyte becomes purple-blue after introducing the ACAT co-additive into the LiNO$_3$-electrolyte (Fig. S4a). The LiPS solution (Li_2S_6) prepared by reacting S and Li_2S is dark yellow (Fig. S4b). By pouring the ACAT powders into the LiPS solution, the color apparently changes from dark yellow to dark green. This phenomenon is very similar to the typical doping reactions of ACAT and PANi.[4,16]

The solubility of ACAT-LiPS complexes was exanimated with the addition of various amounts of ACAT into 1 M LiPS solution. The solution starts to have some suspensions/precipitates when the concentration of ACAT is at 0.07 M. In other words, either the ACAT-LiPS complexes or ACAT reaches their solubility limit in the electrolyte at this concentration.

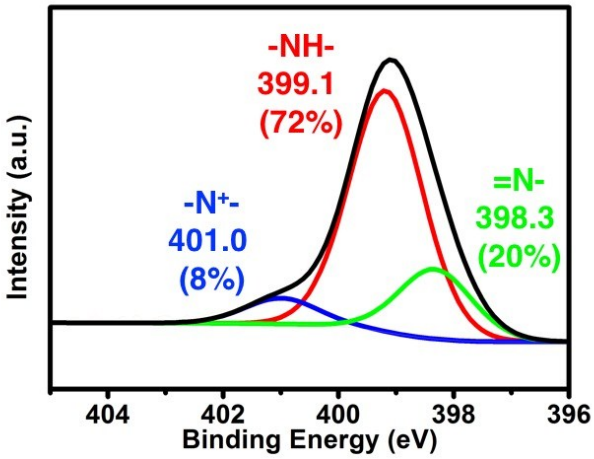

Fig. S5 High-resolution XPS N 1s of ACAT.

Fig. S5 presents the high-resolution N 1s XPS spectrum of the as-synthesized ACAT. The main peak can be decomposed into three peaks. The peak at 393.3 eV is associated with the undoped imine nitrogen.[16–18] The peak at 399.1 eV, on the other hand, corresponds to the amine nitrogen. The peak located at 401.0 eV is related to the positively charged nitrogen (polarons and bipolarons). The protonated nitrogen is attributed to the trace protonated nitrogen from the emeraldine salt state.[16–18]

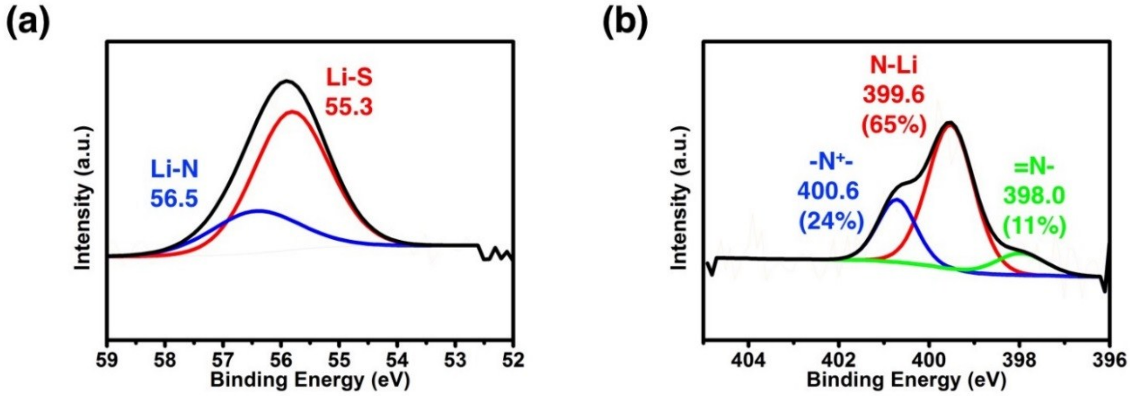

Fig. S6 High-resolution XPS (a) Li 1s and (b) N 1s of the cycled sulfur cathode.

In order to avoid the complete removal of the ACAT-LiPS complexes, the cycled sulfur cathodes were just slightly cleaned with the DOL/DME solution. The rinsed cathodes were investigated by the XPS as shown in Fig. S6. The Li 1s spectrum of the cycled sulfur cathode shows an asymmetric peak extending to the higher binding energy of 56.5 eV, which is attributed to the interactions between the Li positions of LiPS and the nitrogen sites of ACAT

(Fig. S6a).[19–22] The Li-N interactions (399.6 eV) can be observed in the N 1s spectrum of the cycled sulfur cathodes (Fig. S6b).[16] Moreover, the increased area ratio (from 8 % to 24%) of the charged nitrogen implies that ACAT is doped with LiPS.[17,18]

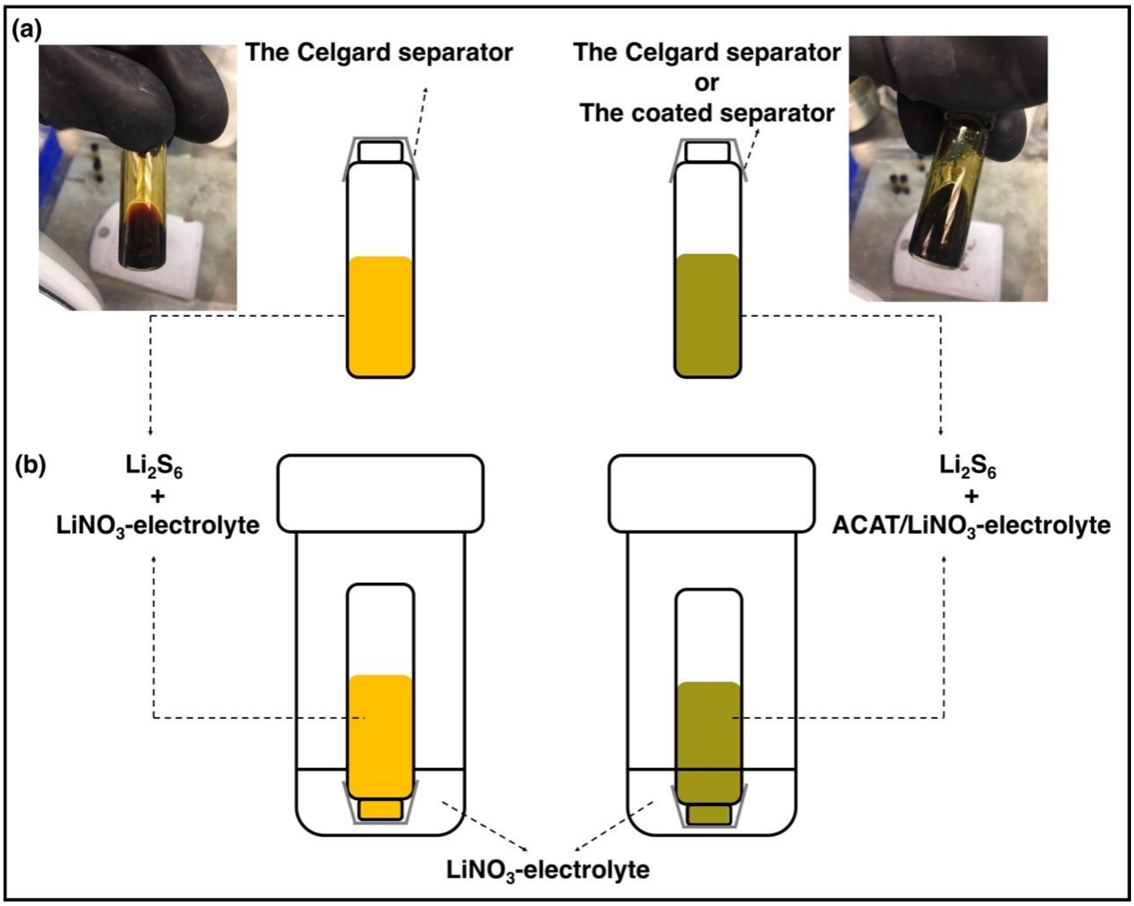

Fig. S7 (a) LiPS/electrolyte mixtures and (b) the permeability tests set-up.

Fig. S7 demonstrates the set-up of the *ex-situ* permeability tests. After immersing for 3 h, the sample using both the ACAT/$LiNO_3$-electrolyte and the carbon-coated separator still remained colorless, indicating the limited crossover of the ACAT-LiPS complexes (the inset in Fig. 2a). Even with the polymeric separators, the solution becomes only slightly greenish-yellow (the inset in Fig. 2b). On the contrary, the dark yellow solution suggests that the severe crossover of LiPS through the polymeric separator occurs in the sample utilizing the $LiNO_3$-electrolyte (the inset in Fig. 2c). The observations provide important evidence that the formed bulky ACAT-LiPS complexes in the ACAT/$LiNO_3$-electrolyte system facilitate the suppression of the LiPS migration due to the size sieving effect. The reduced migration phenomena can be further pronounced by replacing the polymeric separator with the carbon-coated separators.

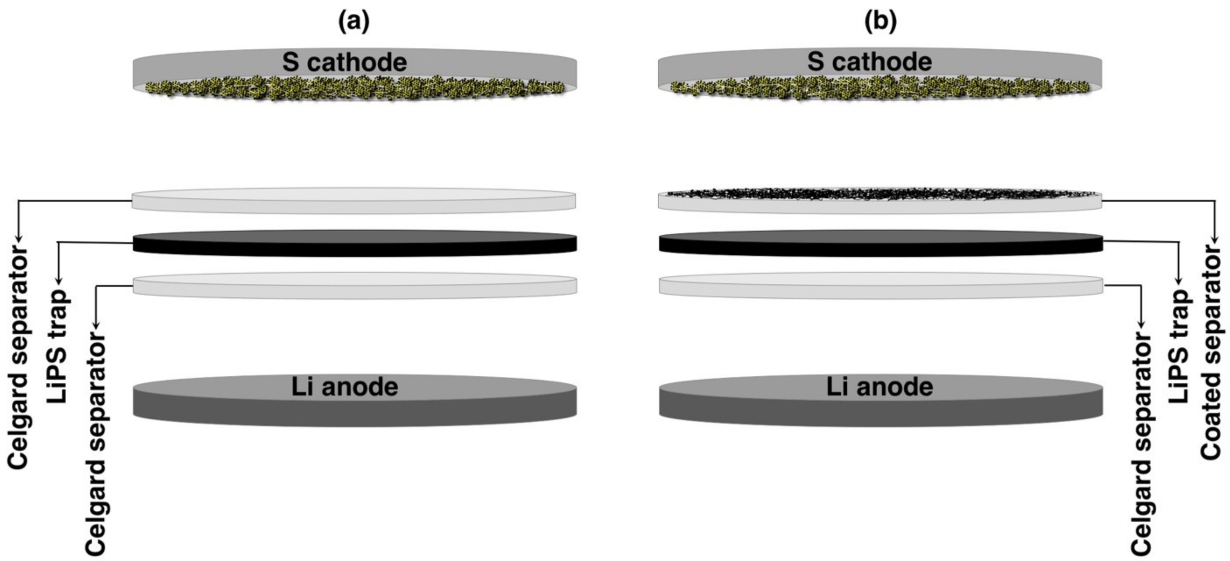

Fig. S8 Configurations of the LiPS-trap cells employing (a) the Celgard separator and (b) the carbon-coated separator.

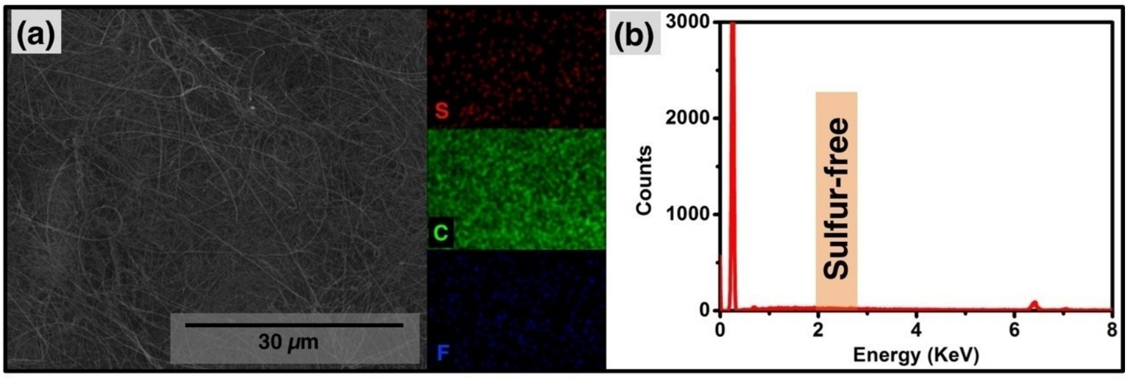

Fig. S9 SEM images and elemental mapping results of the carbon paper used in the LiPS-trap cells.

The configurations of the LiPS-trap cells are shown in Fig. S8. A carbon paper which is originally sulfur-free is inserted between two separators. The carbon papers exhibit intertwined structures with numerous open space between each carbon nanofiber/nanotube (Fig. S9) and therefore have excellent LiPS-trapping capability (65 mg cm^{-2}). Upon cycling, the escaped LiPS from the sulfur cathodes can be completely captured by the inserted carbon papers. Thus, we are able to determine the LiPS-diffusion extents by evaluating the intensity of the sulfur signals.

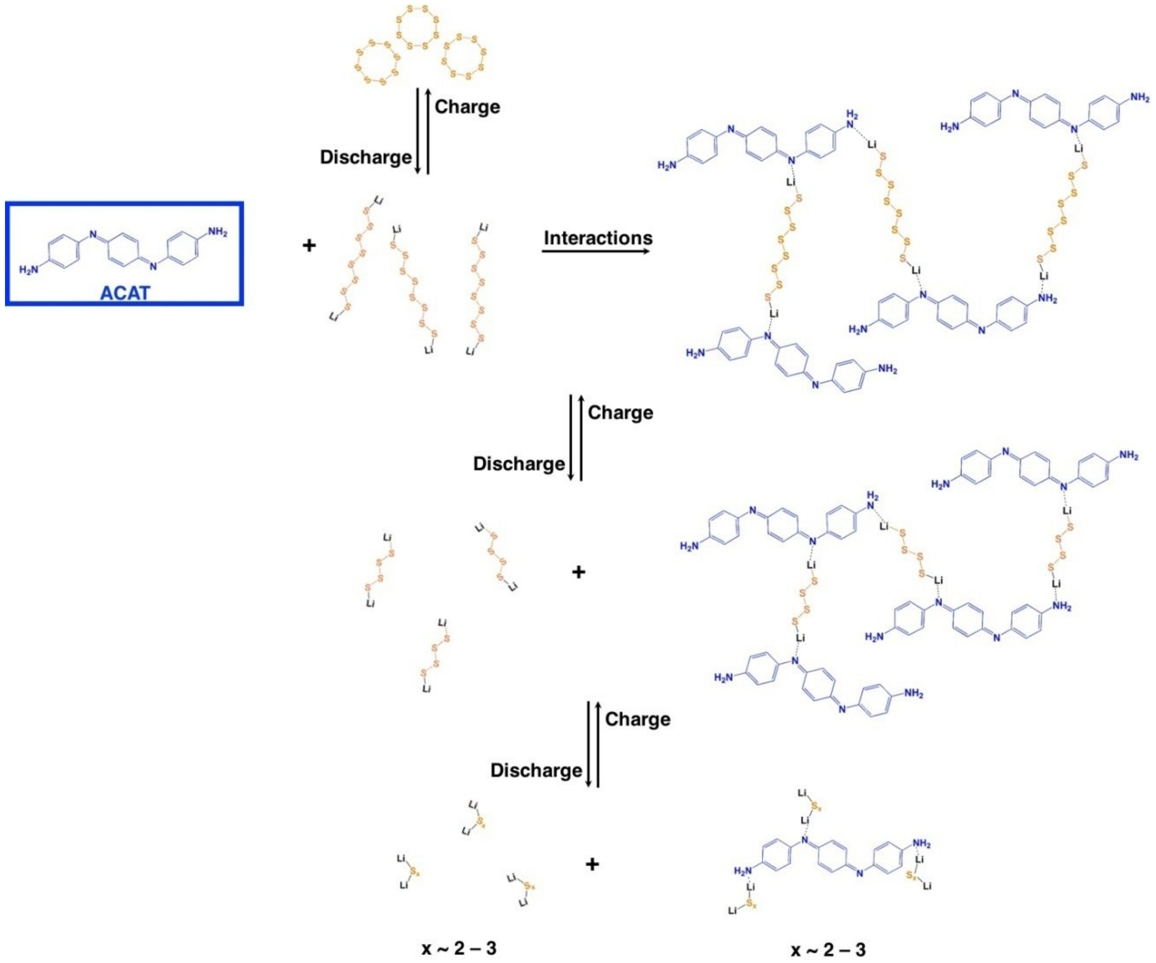

Fig. S10 Proposed redox reactions of the Li-S cells employing the ACAT/$LiNO_3$-electrolyte.

Fig. S10 presents the proposed electrochemical reactions in the Li-S cells employing the ACAT/$LiNO_3$-electrolyte. The octasulfur units (S_8) are reduced to Li_2S_8 in the initial stage (the upper-discharge plateau).[23–25] As the dissolution of linear Li_2S_8 chains occurs in the ACAT/$LiNO_3$-electrolyte, the ACAT molecules interact with the Li_2S_8 chains and then form the ACAT-Li_2S_8 complexes. The Li_2S_8 and ACAT-Li_2S_8 complexes may co-exist in the electrolyte. The further reduction reactions generate the shorter linear LiPS chains and the ACAT-LiPS complexes with shorter oligosulfur units (we used Li_2S_4 as an example in Fig. S10). The continuous discharge step to the lower-discharge plateau results in the further conversion to the insoluble lower-order sulfides (denoted as Li_2S_x; $x = 2 \sim 3$) and the ACAT-LiPS complexes with lower-order LiPS (denoted as ACAT-Li_2S_x; $x = 2 \sim 3$). According to the previous reports, the lower-order sulfides are more soluble in the electrolyte if they are connected to soluble organic segments.[23,26] Similarly, the low-order LiPS mixtures interacting with the highly soluble ACAT compounds (plasticizers) could be considered as the more soluble complexes in the electrolyte.[23] The relatively soluble complexes can somehow alleviate the insoluble sulfide passivation on the cathodes.

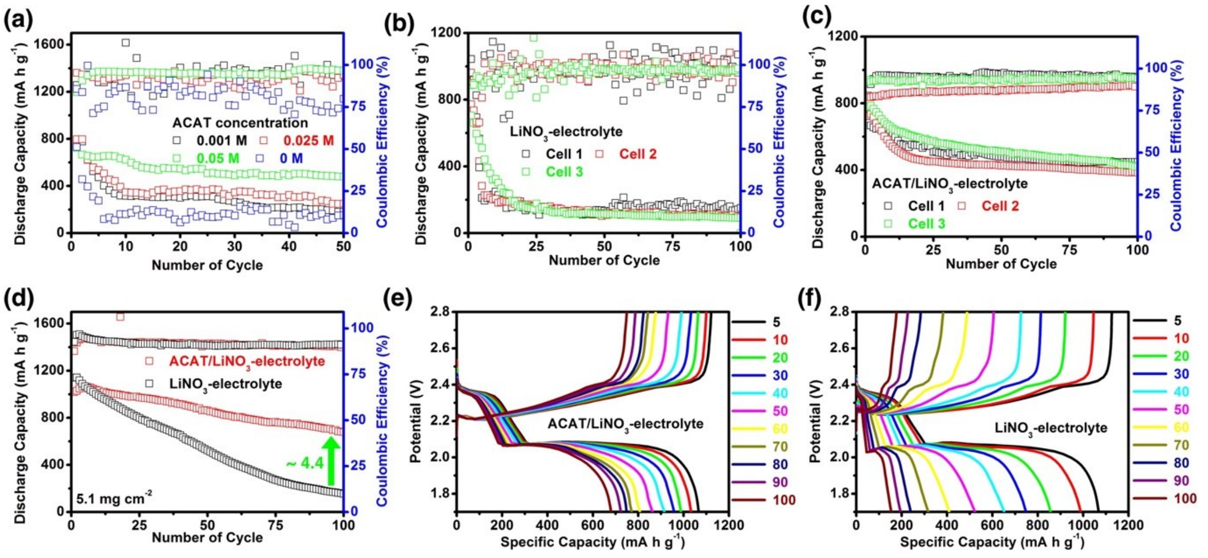

Fig. S11 (a) Effects of the ACAT concentration on the electrochemical performance of the Li-S cells. Reproducibility of the electrochemical performance of the Li-S cells utilizing (b) ACAT/$LiNO_3$-electrolyte and (c) $LiNO_3$-electrolyte. Cells employing the modified cathodes: (d) cyclability and the voltage profiles of the cells employing (e) ACAT/$LiNO_3$-electrolyte and (f) $LiNO_3$-electrolyte.

In Fig. S11a, as the ACAT concentration reaches 0.05 M, it shows a significant improvement in the electrochemical performance, considering that no other protections are involved in the unmodified cell configuration employing pure sulfur cathodes. The electrochemical performances of the cells employing the ACAT/$LiNO_3$-electrolyte and $LiNO_3$-electrolyte are reproducible as shown in Fig. S11b – c.

The modified cathodes with 30 μL of Li_2S_6 solution (~5.1 mg cm^{-2} sulfur) on a highly conductive carbon paper, functionalizing as a porous current collector, were also used to examine the effect of ACAT in ameliorating the electrochemical performance. The cells utilizing the ACAT/$LiNO_3$-electrolyte show *ca.* 4.4 times improvement in the reversible capacity (Fig. 11d). Moreover, the cells utilizing the ACAT/$LiNO_3$-electrolyte exhibit identical discharge/charge curves for 100 cycles, indicating the promising electrochemical performance (Fig. 11e). In contrast, the discharge/charge curves of the cells using the $LiNO_3$-electrolyte continuously shrink during extended cycles, implying the unstoppable LiPS migration and severe inactive sulfide deposition occurring in the cells (Fig. 11f). Accordingly, the electrochemical performances of both the conventional cells and the modified cells confirm the effect of ACAT in suppressing the migration of LiPS during cycling.

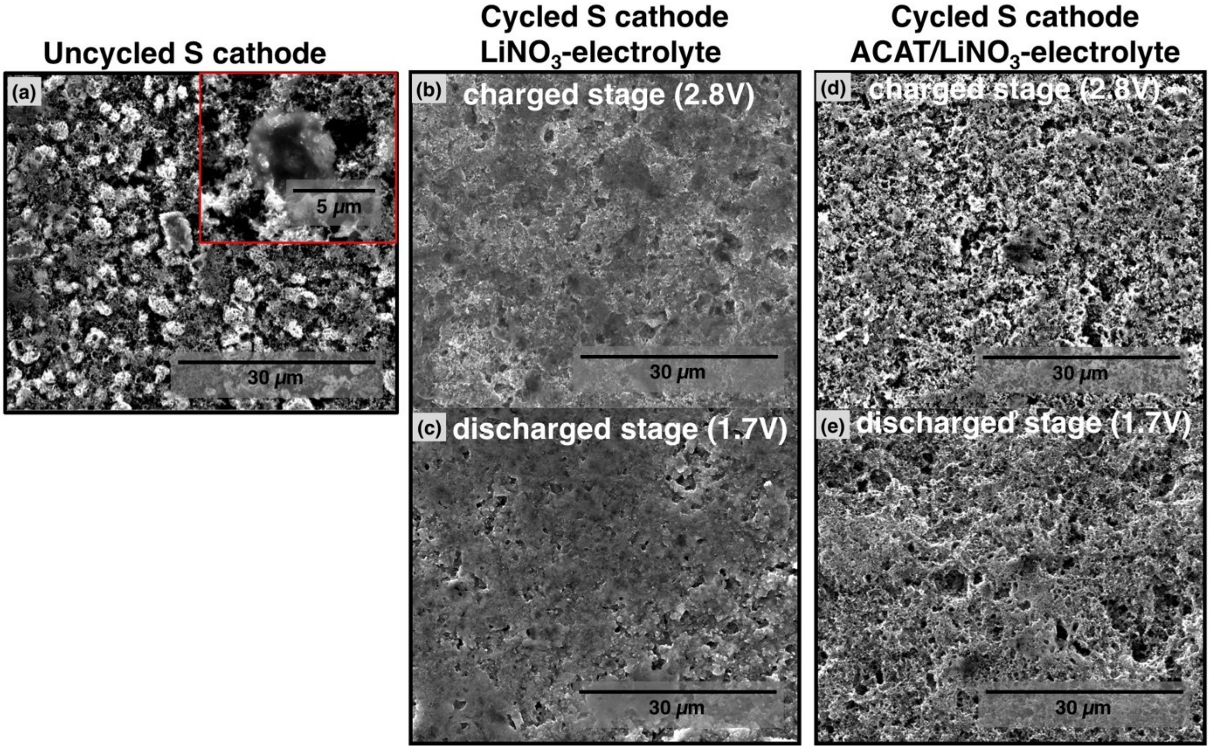

Fig. S12 SEM images of (a) uncycled sulfur cathodes, the cycled sulfur cathodes in the $LiNO_3$-electrolyte (b) at charged state and (c) at discharged state, and the cycled sulfur cathodes in the ACAT/$LiNO_3$-electrolyte (d) at charged state and (e) at discharged state.

The SEM images of the cycled pure sulfur cathodes were used to investigate the suppressed inactive sulfide deposition in the cells employing the ACAT/LiNO3-electrolyte (Fig. S12). The SEM image of the uncycled sulfur cathode shows that the conspicuous S particles (diameters of 5 – 10 µm, as shown in the inset of Fig. S12a) are covered by carbon materials and polymeric binders intimately. The insulating sulfide aggregates, which do not participate in oxidation reactions, accumulate at the surface of the cycled sulfur cathode in the $LiNO_3$-electrolyte system (Fig. S12b – c). The thick irreversible sulfide precipitates diminish the electroactive areas and block ionic transport pathways, leading to an inferior reutilization of the active material and fast capacity fade.[27–30] After cycling in the ACAT/$LiNO_3$-electrolyte, the well-maintained porous structure without the electrochemically irreversible sulfide deposits (Fig. S12d – e) could be explained by the plasticization of the insoluble sulfides. This is similar to the previous result that highly soluble organic compounds, ACAT, act as the plasticizers in the low-order sulfide materials and facilitate an even distribution of the sulfide species.[23] As a result, the well-distributed ACAT-LiPS complexes within the conductive carbon materials enable an efficient utilizations of the active material.

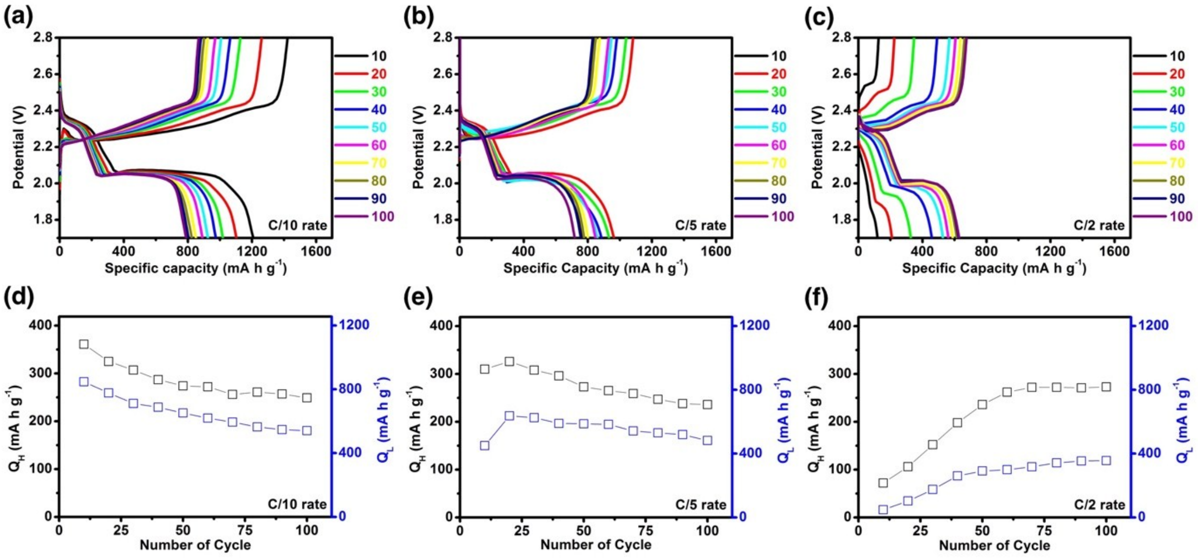

Fig. S13 Voltage profiles and the analysis of Q_H and Q_L with the Li-S cells employing the ACAT/LiNO$_3$-electrolyte and the carbon-coated separators at various cycling rates of (a and d) C/10, (b and e) C/5, and (c and f) C/2 (sulfur loading: 4 mg cm^{-2}).

The ACAT co-additive upgrades the effectiveness of the LiNO$_3$-elecrtrolyte in improving the electrochemical performances of the Li-S cells due to its capability to suppress the migration phenomena. The carbon-coated separators established in our group are able to further enhance the performances.[8–11] Not only does the carbon coating of the coated separators offer an additional sieving layer but also provide a highly conductive framework to reutilize/reactivate the localized active material.

The upper-plateau (Q_H) and lower-plateau discharge capacity (Q_L) are quantitative analyses to determine the LiPS retention extent and redox accessibility.[9,31–33] The upper-discharge plateau principally indexes the degradation of capacity and redox stability of the cells because it reflects the fast reaction kinetics ($S_{8(solid)}$-$LiPS_{(liquid)}$ transition) of the formation and migration of LiPS.[31,32] The lower-discharge plateau, on the other hand, is associated with the sluggish reduction reaction of LiPS to insoluble sulfide species.[9,33] Therefore, the Q_H retention (RQ_H) and Q_L retention (RQ_L) rates, respectively, demonstrate the LiPS stagnation capability and the redox ability. Fig. S13 shows the voltage profiles of the Li-S cells with the carbon-coated separator employing the ACAT/LiNO$_3$-electrolyte at various cycling rates. After 100 cycles, the overlapped upper-discharge plateau with high RQ_H rates suggest the excellent LiPS retention in spite of using the pure sulfur cathodes with a high loading of 4 mg cm^{-2}. The well-retained Q_L values, on the other hand, demonstrate that the cells exhibit a thorough reduction reaction of the localized active material and superior electrochemical reversibility.

An activation process is found to be necessary for the cells at a higher cycling rate such as C/2 rate. Upon cycling at high C-rates, the pure sulfur powders slowly transform to linear LiPS chains, which dissolve into the ACAT/LiNO$_3$-electrolyte and interact with the ACAT molecules, forming the bulky ACAT-LiPS complexes. The dissolved large ACAT-LiPS complexes are confined within the cathode region due to the molecular structural hindrance effects. The stabilized ACAT-LiPS complexes can facilitate the activation processes of bulk sulfur powders.[34] As a consequence, an escalating tendency in the discharge capacity can be observed in the cells at C/5 and C/2 rates. Especially, the cells cycling at the C/2 rate exhibit a relatively long activation process due to the much faster discharge/charge procedures.

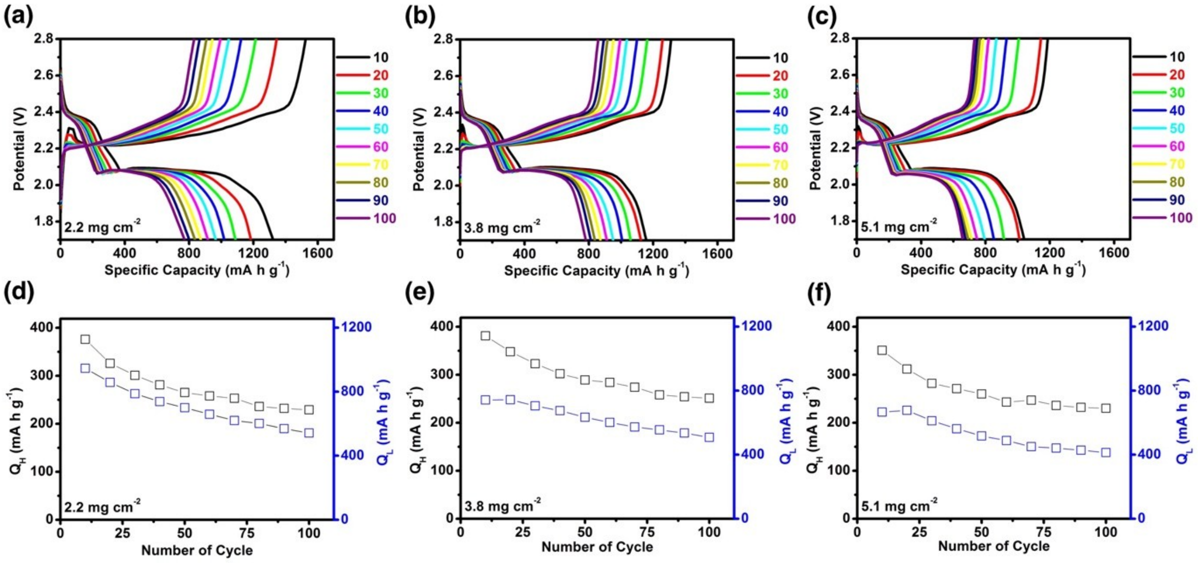

Fig. S14 Voltage profiles and the analysis of Q_H and Q_L with the Li-S cells employing the ACAT/$LiNO_3$-electrolyte and the carbon-coated separators with different active-material loadings of (a and d) 2.2 mg cm^{-2}, (b and e) 3.8 mg cm^{-2}, and (c and f) 5.1 mg cm^{-2}.

The sulfur loading is a critical parameter affecting the electrochemical performance of the Li-S battery. As the loading increases, the unfavorable issues are more pronounced in the Li-S cells. The combination of the ACAT/$LiNO_3$-electrolyte and the carbon-coated separators significantly ameliorates these problems and therefore improves the electrochemical performances despite employing pure sulfur cathodes with increasing sulfur loadings from 2.2 mg cm^{-2} to 5.1 mg cm^{-2}. The voltage profiles of the cells with various loadings at the C/10 rate are shown in Fig. S14. The overlapped discharge/charge curves demonstrate the excellent cycling stability of the cells. The high RQ_H and RQ_L values reflect the outstanding LiPS localization and the promising reutilization of the active materials.

Table S1. Comparisons of the effects of the previous electrolyte additive work.

Electrolyte additives	Effects	Ref.
Lithium nitrate ($LiNO_3$)	Facilitate stable passivation layers containing Li_xNO_y and Li_xSO_y on the surfaces of electrodes.	35–37
Lithium iodine (LiI)	i) Promote the formation of the "protective" layer on the surface of both electrodes. ii) Reduce the activation energy and decrease the overpotential of the Li_2S cathode at the first cycle.	38
Lanthanum nitrate ($La(NO_3)_3$)	The passivation layer contains La_2S_3, Li_2S_2/Li_2S, and Li_xSO_y on the Li anode.	39
Ammonium additives (NH_4NO_3)	i) The NO^{3-} anions assist in the dissociation of crystalline Li_2S. ii) Ammonium additives raise the oxidation kinetics of Li_2S.	40
Dimethyl disulfide (CH_3SSCH_3)a)	Formation of dimethyl polysulfides and organosulfides improves the redox capability and lowers the charge overpotential.	41,42
Phosphorous pentasulfide (P_2S_5)	i) The formation of the highly soluble complexes with P_2S_5 ii) A passivation layer containing Li_3PS_4 on the surface of the Li anode	43
Benzoperyleneimide (BPI)a)	Formation three-dimensional (3D) structure and porous Li_2S depositions	44
Dithiothreitol (DTT)a)	Accelerate the reduction reaction from LiPS to Li_2S by cleaving the -S-S- bonds	45
Biphenyl-4,4'-dithiol (BPD)	Formation of BPD-short chain polysulfide complexes alters the kinetics of the dissolution process.	46
ACAT a)	i) Reduce the migration of LiPS by forming the bulky ACAT-LiPS complexes through the strong interactions ii) Formation of soluble ACAT-LiPS (low-order) complexes	This work

a) $LiNO_3$ is necessary in the electrolyte.

Table S2. Summary of the XPS N 1s spectra of the as-synthesized ACAT, ACAT-LiPS, and the cycled cathode.

	=N- (area ratio)	$-N^+-$ (area ratio)	N-H/Li (area ratio)
As-synthesized ACAT	398.3 (20%)	401.0 (8%)	399.1 (72%)
ACAT-LiPS	398.4 (10%)	400.4 (21%)	399.7 (69%)
Cycled cathode	398.0 (11%)	400.6 (21%)	399.6 (69%)

Table S3. Summary of the analysis of Q_H and Q_L with the Li-S cells.

	Q_H (mA h g^{-1})a)	Q_H (mA h g^{-1})b)	RQ_H (%)	Q_L (mA h g^{-1})a)	Q_L (mA h g^{-1})b)	RQ_L (%)
C/10	361	249	69%	847	540	64%
C/5	310	236	76%	450	482	Activationc)
C/2	72	273	Activationc)	48	356	Activationc)
2.2 mg cm^{-2}	376	229	61%	946	542	57%
3.8 mg cm^{-2}	381	251	66%	742	508	68%

5.1 mg cm^{-2}	351	230	66%	666	413	62%

[a] 10th cycle; [b] 100th cycle; [c] Over 100% retention rates are due to the longer activation processes at higher cycling rates.

Table S4. Electrochemical performance summary.

	Cycling rate	S loading (mg cm^{-2})	S content (%)	Peak capacity (mA h g^{-1})	S utilization rate (%)[a]	Reversible capacity (mA h g^{-1})	Capacity retention (%)[b]	Fading rate (% per day)[c]
ACAT/LiNO$_3$	C/10	4.0	70	1269	76	726[d]	57	0.29
ACAT/LiNO$_3$	C/5	4.0	70	963	58	580[d]	62	0.27
ACAT/LiNO$_3$	C/2	4.0	70	633	38	575[d]	91	0.06
ACAT/LiNO$_3$	C/10	2.2	70	1420	85	590[e]	42	0.29
ACAT/LiNO$_3$	C/10	3.8	70	1270	76	571[e]	45	0.28
ACAT/LiNO$_3$	C/10	5.1	70	1028	61	514[e]	50	0.25

[a] S utilization rate = (peak capacity/1675 mA h g^{-1})*100; [b] capacity retention = (reversible capacity/peak capacity)*100; [c] Fading rate = (peak capacity-reversible capacity)/reversible capacity/the cycle number*100; [d] 150th cycle; [e] 200th cycle.

References

1 C.-J. Weng, C.-H. Chang, C.-W. Peng, S.-W. Chen, J.-M. Yeh, C.-L. Hsu and Y. Wei, *Chem. Mater.*, 2011, **23**, 2075–2083.
2 H.-Y. Huang, T.-C. Huang, J.-C. Lin, J.-H. Chang, Y.-T. Lee and J.-M. Yeh, *Mater. Chem. Phys.*, 2013, **137**, 772–780.
3 K.-Y. Huang, C.-L. Shiu, P.-S. Wu, Y. Wei, J.-M. Yeh and W.-T. Li, *Electrochimica Acta*, 2009, **54**, 5400–5407.
4 C.-J. Weng, Y.-S. Jhuo, K.-Y. Huang, C.-F. Feng, J.-M. Yeh, Y. Wei and M.-H. Tsai, *Macromolecules*, 2011, **44**, 6067–6076.
5 C.-J. Weng, Y.-S. Jhuo, C.-H. Chang, C.-F. Feng, C.-W. Peng, C.-F. Dai, J.-M. Yeh and Y. Wei, *Soft Matter*, 2011, **7**, 10313–10318.
6 Y. Wei, C. Yang and T. Ding, *Tetrahedron Lett.*, 1996, **37**, 731–734.
7 C.-H. Chang, T.-C. Huang, C.-W. Peng, T.-C. Yeh, H.-I. Lu, W.-I. Hung, C.-J. Weng, T.-I. Yang and J.-M. Yeh, *Carbon*, 2012, **50**, 5044–5051.
8 S.-H. Chung and A. Manthiram, *Adv. Mater.*, 2014, **26**, 7352–7357.
9 C.-H. Chang, S.-H. Chung and A. Manthiram, *J. Mater. Chem. A*, 2015, **3**, 18829–18834.
10 C.-H. Chang, S.-H. Chung and A. Manthiram, *Small*, 2016, **12**, 174–179.
11 S.-H. Chung and A. Manthiram, *Adv. Funct. Mater.*, 2014, **24**, 5299–5306.
12 J. Chen, B. Guo, T. W. Eyster and P. X. Ma, *Chem. Mater.*, 2015, **27**, 5668–5677.
13 Y. Wang, H. D. Tran, L. Liao, X. Duan and R. B. Kaner, *J. Am. Chem. Soc.*, 2010, **132**, 10365–10373.
14 A. G. MacDiarmid, *Angew. Chem. Int. Ed.*, 2001, **40**, 2581–2590.
15 A. J. Heeger, *Angew. Chem. Int. Ed.*, 2001, **40**, 2591–2611.
16 P. Jiménez, E. Levillain, O. Alévêque, D. Guyomard, B. Lestriez and J. Gaubicher, *Angew. Chem. Int. Ed.*, 2017, **56**, 1553–1556.
17 K. S. Ryu, K. M. Kim, S.-G. Kang, G. J. Lee, J. Joo and S. H. Chang, *Synth. Met.*, 2000, **110**, 213–217.
18 K. S. Ryu, J. H. Jung, J. Joo and S. H. Chang, *J. Electrochem. Soc.*, 2002, **149**, A478–A482.
19 Z. W. Seh, H. Wang, P.-C. Hsu, Q. Zhang, W. Li, G. Zheng, H. Yao and Y. Cui, *Energy Environ. Sci.*, 2014, **7**, 672–676.
20 L. Ma, H. L. Zhuang, S. Wei, K. E. Hendrickson, M. S. Kim, G. Cohn, R. G. Hennig and L. A. Archer, *ACS Nano*, 2016, **10**, 1050–1059.
21 Q. Pang, J. Tang, H. Huang, X. Liang, C. Hart, K. C. Tam and L. F. Nazar, *Adv. Mater.*, 2015, **27**, 6021–6028.

22 Z. W. Seh, Q. Zhang, W. Li, G. Zheng, H. Yao and Y. Cui, *Chem. Sci.*, 2013, **4**, 3673–3677.

23 A. G. Simmonds, J. J. Griebel, J. Park, K. R. Kim, W. J. Chung, V. P. Oleshko, J. Kim, E. T. Kim, R. S. Glass, C. L. Soles, Y.-E. Sung, K. Char and J. Pyun, *ACS Macro Lett.*, 2014, **3**, 229–232.

24 J. J. Griebel, R. S. Glass, K. Char and J. Pyun, *Top. Vol. Polym. Chem.*, 2016, **58**, 90–125.

25 P. T. Dirlam, R. S. Glass, K. Char and J. Pyun, *J. Polym. Sci. Part Polym. Chem.*, 2017, **55**, 1635–1668.

26 W. J. Chung, J. J. Griebel, E. T. Kim, H. Yoon, A. G. Simmonds, H. J. Ji, P. T. Dirlam, R. S. Glass, J. J. Wie, N. A. Nguyen, B. W. Guralnick, J. Park, SomogyiÁrpád, P. Theato, M. E. Mackay, Y.-E. Sung, K. Char and J. Pyun, *Nat Chem*, 2013, **5**, 518–524.

27 S.-E. Cheon, K.-S. Ko, J.-H. Cho, S.-W. Kim, E.-Y. Chin and H.-T. Kim, *J. Electrochem. Soc.*, 2003, **150**, A796–A799.

28 S.-E. Cheon, K.-S. Ko, J.-H. Cho, S.-W. Kim, E.-Y. Chin and H.-T. Kim, *J. Electrochem. Soc.*, 2003, **150**, A800–A805.

29 L. Yuan, X. Qiu, L. Chen and W. Zhu, *J. Power Sources*, 2009, **189**, 127–132.

30 S.-E. Cheon, J.-H. Cho, K.-S. Ko, C.-W. Kwon, D.-R. Chang, H.-T. Kim and S.-W. Kim, *J. Electrochem. Soc.*, 2002, **149**, A1437–A1441.

31 X. Yang, N. Yan, W. Zhou, H. Zhang, X. Li and H. Zhang, *J. Mater. Chem. A*, 2015, **3**, 15314–15323.

32 X. Yang, Y. Yu, N. Yan, H. Zhang, X. Li and H. Zhang, *J. Mater. Chem. A*, 2016, **4**, 5965–5972.

33 S.-H. Chung, R. Singhal, V. Kalra and A. Manthiram, *J. Phys. Chem. Lett.*, 2015, **6**, 2163–2169.

34 S.-H. Chung, P. Han and A. Manthiram, *ACS Appl. Mater. Interfaces*, 2016, **8**, 4709–4717.

35 S. S. Zhang, *Electrochimica Acta*, 2012, **70**, 344–348.

36 S. S. Zhang, *J. Power Sources*, 2016, **322**, 99–105.

37 X. Liang, Z. Wen, Y. Liu, M. Wu, J. Jin, H. Zhang and X. Wu, *J. Power Sources*, 2011, **196**, 9839–9843.

38 F. Wu, J. T. Lee, N. Nitta, H. Kim, O. Borodin and G. Yushin, *Adv. Mater.*, 2015, **27**, 101–108.

39 S. Liu, G.-R. Li and X.-P. Gao, *ACS Appl. Mater. Interfaces*, 2016, **8**, 7783–7789.

40 H. Pan, K. S. Han, M. Vijayakumar, J. Xiao, R. Cao, J. Chen, J. Zhang, K. T. Mueller, Y. Shao and J. Liu, *ACS Appl. Mater. Interfaces*, 2017, **9**, 4290–4295.

41 S. Chen, F. Dai, M. L. Gordin, Z. Yu, Y. Gao, J. Song and D. Wang, *Angew. Chem. Int. Ed.*, 2016, **55**, 4231–4235.

42 S. Chen, Y. Gao, Z. Yu, M. L. Gordin, J. Song and D. Wang, *Nano Energy*, 2017, **31**, 418–423.

43 Z. Lin, Z. Liu, W. Fu, N. J. Dudney and C. Liang, *Adv. Funct. Mater.*, 2013, **23**, 1064–1069.

44 L. C. H. Gerber, P. D. Frischmann, F. Y. Fan, S. E. Doris, X. Qu, A. M. Scheuermann, K. Persson, Y.-M. Chiang and B. A. Helms, *Nano Lett.*, 2016, **16**, 549–554.

45 W. Hua, Z. Yang, H. Nie, Z. Li, J. Yang, Z. Guo, C. Ruan, X. Chen and S. Huang, *ACS Nano*, 2017, **11**, 2209–2218.

46 H.-L. Wu, M. Shin, Y.-M. Liu, K. A. See and A. A. Gewirth, *Nano Energy*, 2017, **32**, 50–58.